Electronic, Structural, and Mechanical Properties of SiO_2 Glass at High Pressure Inferred from its Refractive Index

Sergey S. Lobanov[1,2,*] Sergio Speziale,[1] Björn Winkler,[3] Victor Milman[4] Keith Refson,[5] and Lukas Schifferle[1,2]
[1]Deutsches GeoForschungsZentrum GFZ, Telegrafenberg, 14473 Potsdam, Germany
[2]Institut für Geowissenschaften, Universität Potsdam, Karl-Liebknecht-Str. 24-25, Golm 14476, Germany
[3]Institut für Geowissenschaften, Goethe-Universität Frankfurt, Altenhöferallee 1, 60438 Frankfurt am Main, Germany
[4]Dassault Systèmes BIOVIA, 334 Science Park, Cambridge CB4 0WN, United Kingdom
[5]ISIS Facility, Rutherford Appleton Laboratory, Chilton, Didcot, Oxfordshire OX11 0QX, United Kingdom

(Received 22 April 2021; revised 29 November 2021; accepted 23 December 2021; published 17 February 2022)

We report the first direct measurements of the refractive index of silica glass up to 145 GPa that allowed quantifying its density, bulk modulus, Lorenz-Lorentz polarizability, and band gap. These properties show two major anomalies at ~10 and ~40 GPa. The anomaly at ~10 GPa signals the onset of the increase in Si coordination, and the anomaly at ~40 GPa corresponds to a nearly complete vanishing of fourfold Si. More generally, we show that the compressibility and density of noncrystalline solids can be accurately measured in simple optical experiments up to at least 110 GPa.

DOI: 10.1103/PhysRevLett.128.077403

The physical properties and the structure of noncrystalline silica are of central importance in solid-state physics and material sciences because SiO_2 is a prototypical glass former and a dominant component of many industrial glasses. Pure vitreous silica, in particular, has been the research focus of numerous studies aimed at understanding and predicting the physical behavior of more complex SiO_2-rich glasses [1–4]. In geophysics, it is liquid silica that is of special importance due to the high SiO_2 content (40–80 mol%) of virtually all terrestrial magmas. Silica-rich liquids played a key role in the differentiation of the early Earth [5] and may still be present near the core-mantle boundary at the depth of ~2900 km [6,7], where the pressure (P) and temperature (T) are very high (136 GPa/ ~ 4000 K). Deciphering the physical properties of SiO_2-rich melts as a function of P and T is thus key to understanding Earth's evolution and the nature of present-day low seismic velocity zones at the base of the mantle [8]. Among the relevant physical properties of melts, their density and viscosity are of primary geophysical importance because they determine the ability of magmas to rise or sink. These two properties are linked to the compressibility and structure of silica-rich melts [9], which remain largely inaccessible to direct probing at deep mantle conditions [10,11]. Silica-bearing liquids, however, present structural similarities to corresponding glasses [12,13], rendering the latter convenient and appropriate proxies of the molten state.

The compressibility of silica glass has been reported to ~10 [14], ~55 [15], and 110 GPa [16] with densities agreeing within the uncertainty at overlapping pressures. The density of SiO_2 glass roughly doubles in the pressure range from 1 atm (2.2 g/cm^3) to 40 GPa (~4.45 g/cm^3). At $P > 40$ GPa, the compressibility of silica glass decreases gradually and at $P > 60$ GPa the glass density approaches that of stishovite and of $CaCl_2$-structured SiO_2 [16], the stable crystalline forms of SiO_2 with ^{VI}Si (sixfold Si). The emergence of ^{VI}Si in dense silica glass has been established by a variety of spectroscopic and structural probes [1,2,15,17–28] as well as *ab initio* computations [29,30]. In this Letter we report on the optical refractive index and its wavelength-dispersion, density, compressibility, Lorenz-Lorentz polarizability, and band gap of fused silica up to $P > 110$ GPa that provide new insights into the structural evolution and transport properties of silica glass with pressure.

The index of refraction of fully compacted and optically transparent silica glass was measured in diamond anvil cells (DACs) using the reflectivity method [31–34] with a broadband (supercontinuum) laser as a probe. See the Supplemental Material [35] for full technical details. This approach is based on the Fresnel law of refraction which relates the reflectance of the diamond-sample interface ($R_{\text{dia-sam}}$) to the refractive indices of diamond (n_{dia}) and sample (n_{sam}). For perpendicularly incident light

$$R_{\text{dia-sam}} = \frac{(n_{\text{sam}} - n_{\text{dia}})^2}{(n_{\text{sam}} + n_{\text{dia}})^2}. \quad (1)$$

The measured reflected signal contains contributions from the two diamond-sample interfaces (I_1 *and* I_2) which are related to $R_{\text{dia-sam}}$:

$$\frac{I_1 + I_2}{I_0} = R_{\text{dia-sam}}^3 - 2R_{\text{dia-sam}}^2 + 2R_{\text{dia-sam}}, \quad (2)$$

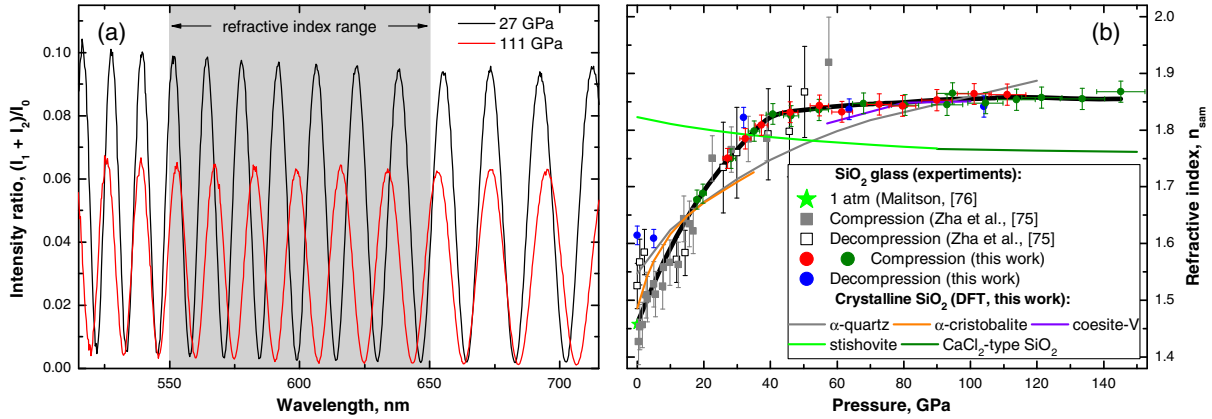

FIG. 1. (a) Intensity ratio spectra ($[I_1 + I_2]/I_0$) at 27 (black) and 111 GPa (red). The gray box depicts the spectral range used to evaluate the refractive index. (b) Refractive index of silica glass measured in this work. The thick black line is a guide to the eye. Previous data on the index of silica glass are from Refs. [75,76]. Results of our own DFT computations [35] of the refractive indices of crystalline SiO_2 phases are shown as continuous curves and color coded as labeled. Pressure was measured by the diamond Raman edge method and the relative pressure uncertainty is ±5% [35,77].

where I_0 is the probe intensity impinging onto the upstream diamond-sample interface (see Fig. S1 in Ref. [35] for graphical definitions). The derivation of Eq. (2) as well as details on the spectroscopic determination of the intensity ratio ($[I_1 + I_2]/I_0$) are provided in the Supplemental Material [35]. Briefly, the intensity ratio is averaged over the 550–650 nm spectral range [Fig. 1(a)] to obtain a single value which is used to solve Eq. (2) for $R_{\text{dia-sam}}$. Then, by solving Eq. (1) for n_{sam} at a fixed $n_{\text{dia}} = 2.418$ [74], we obtain the refractive index of silica glass at 600 nm. The assumption of the pressure-independent index of diamond is appropriate as discussed in Ref. [35].

On compression, the refractive index of silica glass increases rapidly up to ~40 GPa [Fig. 1(b)] in agreement with the literature data based on Brillouin scattering measurements [75]. The pressure derivative of the index abruptly reduces at $P \sim 40$ GPa but remains positive up to 145 GPa. The increase in refractive index is reversible upon decompression to ~30 GPa, but at $P <$ ~30 GPa, the index of decompressed glass is systematically higher than that measured on compression. The index of silica glass decompressed from 145 GPa to 1 atm is roughly equal to that of α-quartz, suggesting an irreversible densification, and transition from a cristobalitelike (precompression) to quartzlike (postcompression) tetrahedral network, consistent with earlier studies [2,14,22,75,78–82].

In one of the compression runs we analyzed the fringe spacing of the intensity ratio spectra (Fig. S3) to obtain the wavelength dispersion of the refractive index at 500–850 nm (Fig. S4 [35]). The index dispersion averaged over 500–850 nm increases by ~80% upon compression from 1 atm to ~37 GPa but decreases at higher pressures by ~13% up to 111 GPa (Fig. S5). We further analyzed the index dispersion using the single-oscillator model of Wemple and DiDomenico [35,83]. From the fitted oscillator energy E_0 we estimate the value of the band gap $E_g = 1.5E_0$ [83] which is constant and equal to 8.03 (±0.04) eV in the range $27 < P < 37$ GPa and then linearly increases up to 8.8 (±0.2) eV at 111 GPa (Fig. S6). This behavior is qualitatively consistent with theoretical predictions [30,84].

To gain structural insights we compare the refractive index of silica glass to that of α-cristobalite and α-quartz (low-density polymorphs of SiO_2), as well as coesite-V [85], stishovite, and the $CaCl_2$ phase of SiO_2 (high-density polymorphs). The indices of these phases were computed from first principles as described in Ref. [35]. The refractive index of α-cristobalite at 1 atm is only ~2% larger than that of the glass and increases at a comparable rate up to ~10 GPa [Fig. 1(b)] [75], likely due to the structural similarities and high compressibility of their SiO_4 networks [86,87]. At $P > 15$ GPa, the index of α-cristobalite becomes lower than that of silica glass due to the decrease in its pressure derivative at ~10 GPa (Fig. S10). This observation hints that the structural similarity between α-cristobalite and the glass is preserved in the limit of $P <$ ~10 GPa but is lost at higher pressure. The refractive index of coesite-V, a metastable polymorph of SiO_2 with both ^{V}Si (37.5%) and ^{VI}Si (62.5%) [85], is nearly independent of P at 60–100 GPa and is similar to that of the glass. The indices of stishovite and $CaCl_2$ phase have a negative pressure dependence and are systematically lower than that of the glass at $P > 40$ GPa.

Our refractive index data allow exploring the compressibility of silica glass. In one experiment without the pressure transmitting medium, the absolute volume of silica glass was determined by directly measuring the thickness and area of a fully compacted sample at $P >$ ~27 GPa [35]. The spacing of the interference extrema in the intensity ratio spectra [Fig. 1(a)], which are formed due to the DAC

cavity being a Fabry-Perot interferometer, yields the product of sample thickness and refractive index. Using our experimentally determined refractive index we obtained the sample thickness at its center and ~5 μm away from the gasket edge (Fig. S2 and Fig. S7A). The uncertainty in sample thickness measured at different positions is that of the refractive index (~1%). To obtain the area of the sample, we photographed the DAC cavity in transmitted light under fixed illuminating conditions and camera settings. Automated finding of all the pixels brighter than a fixed threshold yielded the sample area (Fig. S7B) with an uncertainty of ~1.5% [35]. The product of averaged sample thickness and area yielded the volume with an uncertainty of ~3.2% at 27 GPa which decreases to ~2.6% at pressures between 55 and 111 GPa [35].

The sample volume (V) decreases by ~27% upon compression from ~27 to ~111 GPa, as recorded in the experiments without pressure medium (Fig. S9). These P-V data can be converted to density if the density at a reference pressure (e.g., 27 GPa) is known. The available reports on density [15,16] can provide such a reference. Here, however, we independently measured the density of a thin (~8 μm) doubly polished silica glass slab, gold coated on one side, up to ~30 GPa in a DAC with argon as a pressure medium [35]. The uncoated side of the slab was in direct contact with one of the anvils. The interference spectra, measured by reflecting the broadband probe from the glass-gold interface, yielded slab thicknesses utilizing the pressure dependence of silica glass refractive index based on the present measurements and the reference value at ambient pressure [76] (Fig. S10). The evolution of the slab thickness with P yielded linear strain along the compression axis while linear strain perpendicular to the compression axis (in the radial direction) was extracted from the optical photographs of the DAC sample chamber. The evolution of the slab volume yielded the density of silica glass up to ~30 GPa by accepting the value of 2.2 g/cm^3 at 1 atm. The densities measured in the run with argon pressure medium are plotted in Fig. 2 (inset). Using the density of 3.9 g/cm^3 measured at 27 GPa in the run performed in an argon pressure medium as a reference, we convert the volume data measured in experiments without pressure medium to absolute density (Fig. 2). The agreement with the previous reports on silica glass density [14–16] is within the error bars.

The compression curve of silica glass has a slope similar to that of α-cristobalite at $P < \sim 10$ GPa (Fig. 2 inset). The glass, however, retains its high compressibility up to ~40 GPa whereas α-cristobalite and α-quartz are less compressible at $P > \sim 10$ GPa. These observations indicate that compression mechanisms are being activated in silica glass at $P \sim 10$ GPa that are not available in α-cristobalite and α-quartz: specifically, the production of ^{V}Si and ^{VI}Si from ^{IV}Si [23]. Our density data thus suggest that the coordination of Si is four up to $P \sim 10$ GPa, in agreement

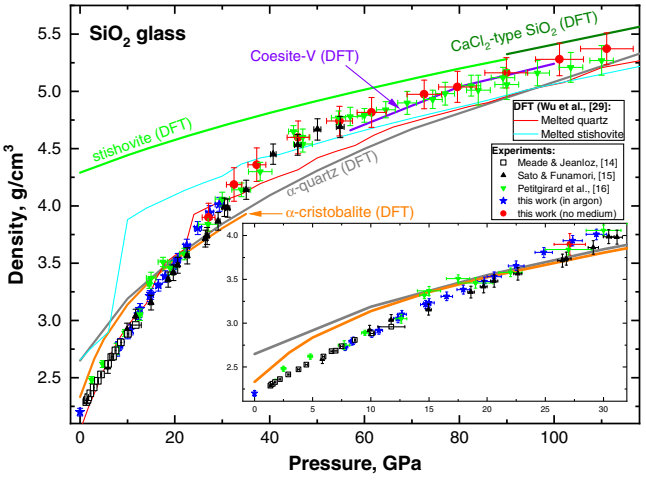

FIG. 2. Silica glass density determined in the experiment with Ar pressure medium (blue stars) and without pressure medium (red circles). Previous experimental data are plotted as empty squares [14], black triangles [15], and green [16] triangles. Thin blue and red curves are two models of silica glass density from Ref. [29]. Our own computations of the density of α-cristobalite (orange), α-quartz (gray), coesite-V (violet), stishovite (light green), and the $CaCl_2$-type SiO_2 (dark green). Inset: Enlarged low-pressure region.

with the previous studies of dense silica glass structure [15,17,20,24]. The onset of increase in silicon coordination at $P \sim 10$ GPa is also supported by the refractive index data discussed above. The densities converted to Eulerian finite strain have been analyzed with standard methods to model the high-pressure density evolution of SiO_2 glass within the framework of the finite strain equation of state [35]. The Eulerian strain analysis reveals a sequence of deviations from linear compression at $P \sim 10 - 13$, ~25 (subtle), and ~40 GPa (Fig. S12). Fused silica shows a distinct high-pressure softening with a minimum of the bulk modulus at ~25–30 GPa (Fig. S16). At $P > 40$ GPa the glass becomes more incompressible and its compression behavior is linear (Fig. S12 [35]).

The density of silica glass at $P > 40$ GPa progressively approaches that of the stable sixfold-coordinated crystalline SiO_2 (Fig. 2), which has been invoked as evidence of completed transition to stishovitelike local structure with ^{VI}Si [15]. However, the compressibility of the glass at $P >$ 40 GPa is still higher than that of stishovite. In addition, the pressure derivatives of the refractive indices of silica glass and stishovite have opposite signs (Fig. 1(b)]. The ongoing increase in Si coordination from ^{V}Si to ^{VI}Si and, possibly, ^{VII}Si in the glass is a viable explanation of both these observations.

To gain further insights into Si coordination we estimated its average value $\langle N_c \rangle$, using the measured wavelength dispersion of the refractive index via the empirical relation $\langle N_c \rangle \sim (E_d/\beta)$ [35]. Here, E_d is the fitted oscillator strength and β is an empirical parameter that reflects the

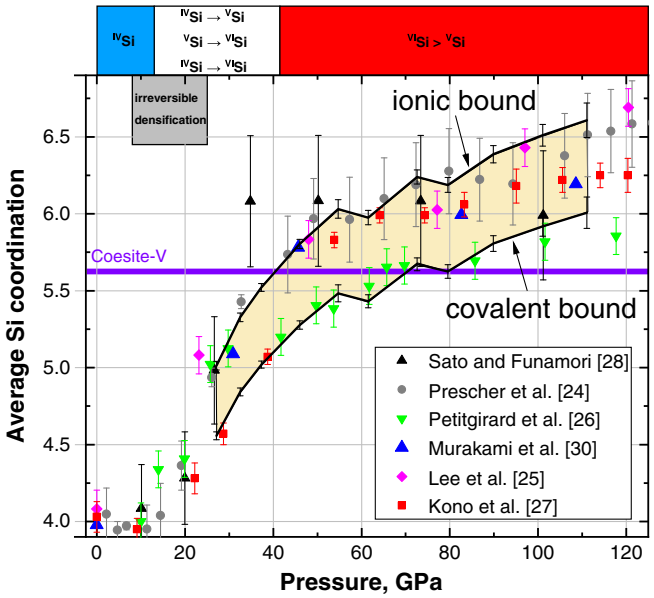

FIG. 3. Bounds to the average coordination of Si in SiO_2 glass at high pressures based on the single-oscillator fit to the wavelength dispersion of the silica glass refractive index (shaded region between the black lines with error bars) [35]. The pressure range of irreversible densification is from Refs. [79,82].

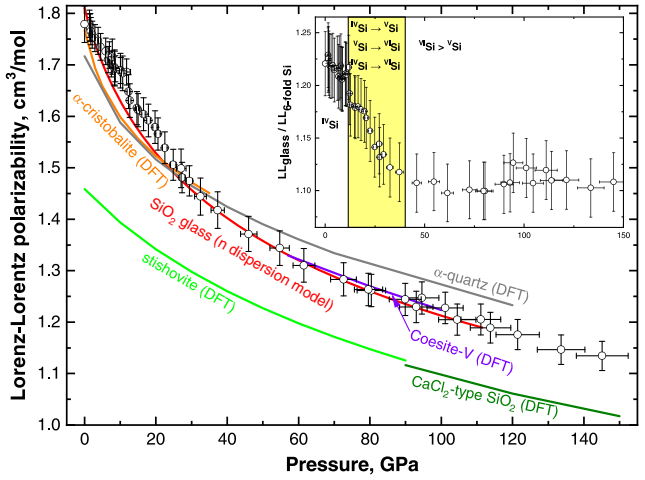

FIG. 4. Lorenz-Lorentz (α_{LL}) polarizability of silica glass (white circles), α-cristobalite (orange line), α-quartz (gray), coesite-V (violet), stishovite (light green), and $CaCl_2$-type SiO_2 (dark green) evaluated using Eq. (3). For silica glass we used the density data of Ref. [14] ($P < 13$ GPa), our own results (7–111 GPa), and their linear extrapolation (111–145 GPa). The red curve is an independent model of silica glass polarizability that is solely based on the measured refractive index dispersion and densities at $46 < P < 111$ GPa [35]. Inset: The ratio of α_{LL} of silica glass to that of crystalline forms of SiO_2 with ^{VI}Si.

ionic or covalent bonding character suggested by Wemple and DiDomenico [83]. Although the character of the Si—O bond at high pressure is unknown, the bounds we obtain from the Wemple-DiDomenico analysis (albeit qualitative) contain most of the extant data on $\langle N_c \rangle$ in SiO_2 glass in the pressure range between 30 and 110 GPa (Fig. 3). The ionic and covalent bounds of our model intersect the value of coesite-V (i.e., 5.6) at ~40 and ~70 GPa, respectively. The average Si coordination inferred in Refs. [24,25] plot close to the ionic bound, suggesting that the Si—O bond in silica glass is largely ionic. By the same logic, the results of Ref. [26] suggest a predominantly covalent character of the Si—O bond.

To link the refractive index and density data to electronic properties, we evaluated the Lorenz-Lorentz (LL) polarizability (α_{LL}):

$$\alpha_{LL} = \frac{1}{\rho}\frac{(n^2-1)}{(n^2+2)}\frac{3M}{4\pi}, \tag{3}$$

with density (ρ), optical refractive index (n), and molecular weight (M) of all the SiO_2 phases considered here. The primary observation is that the polarizability of silica glass decreases approximately linearly up to ~30 GPa (Fig. 4) due to its high compressibility. This is consistent with molecular dynamics simulations that showed that the probabilities of $^{IV}Si \rightarrow {}^{V}Si$ and $^{IV}Si \rightarrow {}^{VI}Si$ transitions peak at $P \sim 10$–30 GPa [23]. We surmise, therefore, that the fraction of ^{IV}Si in the glass structure remains significant at $P = 10$–30 GPa. The polarizability slope becomes less negative at ~30–40 GPa, and at $P >$ ~40 GPa the slope is the same as that of stishovite and $CaCl_2$-type SiO_2. The observed trend of the LL polarizability at $46 < P < 111$ GPa is independently reproduced through the proportionality between the density dependence of polarizability and that of the model single oscillator energy E_0 [35].

The inset of Fig. 4 emphasizes the relatively sharp crossover in the slope of α_{LL} to that of crystalline phases with ^{VI}Si. We attribute the rapid change of slope at ~40 GPa to almost complete vanishing of ^{IV}Si in the glass, which is also supported by the Eulerian finite strain analysis of the density data (Fig. S14), consistent with computational studies that found that the fraction of ^{IV}Si is less than 10% at $P >$ ~40 GPa [23,29,30]. The vanishing of ^{IV}Si in the structure of silica glass causes a decrease of its compressibility at $P >$ ~40 GPa and implies the transition to a less effective densification by $^{V}Si \rightarrow {}^{VI}Si$ and/or contraction of SiO_6-octahedra. However, the abundance of ^{V}Si in silica glass at $P >$ ~40 GPa is unclear. Computational studies disagree on the abundance of ^{V}Si proposing that it falls below 10% at $P >$ ~60 [23,30] or at $P > 120$ GPa [29]. The emergence of ^{VII}Si at the level of >10% is also controversial (at 46–83 [30] vs 180 GPa [29]). Our results support the emergence of ^{VII}Si at 60–100 GPa because the average Si coordination exceeds six at greater pressures (Fig. 3). Overall, the refractive index and density data on silica glass reinforce the view of a continuously evolving Si coordination number at $P > 40$ GPa.

To the best of our knowledge, only the densities of SiO_2, $MgSiO_3$, and GeO_2 glasses have been measured to pressures exceeding 100 GPa [16,88,89]. The glass density in these previous studies was derived from the evolution of the sample volume with pressure as quantified from the x-ray absorbance of the glass in two mutually perpendicular directions, which requires tightly focused synchrotron x rays and x-ray transparent gaskets (e.g., Be). In this Letter we demonstrated that the evolution of the sample volume and density of transparent glasses can be accurately measured up to at least 110 GPa by optical techniques, i.e., outside synchrotron facilities. Therefore, the reported developments open new research avenues to study mechanical and electronic properties of noncrystalline solids with vast implications in materials sciences and geophysics. In addition, such information may serve to benchmark computational studies of transport properties of glasses and melts at extreme conditions.

S. S. L. and L. S. acknowledge the support of the Helmholtz Young Investigators Group CLEAR (VH-NG-1325). B. W. is grateful for support through the BIOVIA Science Ambassador program.

*Corresponding author.
slobanov@gfz-potsdam.de

[1] R. J. Hemley, H. K. Mao, P. M. Bell, and B. O. Mysen, Raman Spectroscopy of SiO_2 Glass at High Pressure, Phys. Rev. Lett. **57**, 747 (1986).
[2] Q. Williams and R. Jeanloz, Spectroscopic evidence for pressure-induced coordination changes in silicate glasses and melts, Science **239**, 902 (1988).
[3] P. F. McMillan, B. T. Poe, P. Gillet, and B. Reynard, A study of SiO_2 glass and supercooled liquid to 1950 K via high-temperature Raman spectroscopy, Geochim. Cosmochim. Acta **58**, 3653 (1994).
[4] L. B. Skinner, C. J. Benmore, J. K. R. Weber, M. C. Wilding, S. K. Tumber, and J. B. Parise, A time resolved high energy x-ray diffraction study of cooling liquid SiO_2, Phys. Chem. Chem. Phys. **15**, 8566 (2013).
[5] S. Labrosse, J. W. Hernlund, and N. Coltice, A crystallizing dense magma ocean at the base of the Earth's mantle, Nature (London) **450**, 866 (2007).
[6] Q. Williams and E. J. Garnero, Seismic evidence for partial melt at the base of Earth's mantle, Science **273**, 1528 (1996).
[7] R. Nomura, K. Hirose, K. Uesugi, Y. Ohishi, A. Tsuchiyama, A. Miyake, and Y. Ueno, Low core-mantle boundary temperature inferred from the solidus of pyrolite, Science **343**, 522 (2014).
[8] E. J. Garnero, A. K. McNamara, and S. H. Shim, Continent-sized anomalous zones with low seismic velocity at the base of Earth's mantle, Nat. Geosci. **9**, 481 (2016).
[9] A. Majumdar, M. Wu, Y. M. Pan, T. Iitaka, and J. S. Tse, Structural dynamics of basaltic melt at mantle conditions with implications for magma oceans and superplumes, Nat. Commun. **11**, 4815 (2020).
[10] P. D. Asimow and T. J. Ahrens, Shock compression of liquid silicates to 125 GPa: The anorthite-diopside join, J. Geophys Res. **115**, B10209 (2010).
[11] C. Sanloup, J. W. E. Drewitt, Z. Konopkova, P. Dalladay-Simpson, D. M. Morton, N. Rai, W. van Westrenen, and W. Morgenroth, Structural change in molten basalt at deep mantle conditions, Nature (London) **503**, 104 (2013).
[12] B. B. Karki, D. Bhattarai, and L. Stixrude, First-principles simulations of liquid silica: Structural and dynamical behavior at high pressure, Phys. Rev. B **76**, 104205 (2007).
[13] D. B. Ghosh, B. B. Karki, and L. Stixrude, First-principles molecular dynamics simulations of $MgSiO_3$ glass: Structure, density, and elasticity at high pressure, Am. Mineral. **99**, 1304 (2014).
[14] C. Meade and R. Jeanloz, Frequency-dependent equation of state of fused silica to 10 GPa, Phys. Rev. B **35**, 236 (1987).
[15] T. Sato and N. Funamori, Sixfold-Coordinated Amorphous Polymorph of SiO_2 under High Pressure, Phys. Rev. Lett. **101**, 255502 (2008).
[16] S. Petitgirard *et al.*, SiO_2 Glass Density to Lower-Mantle Pressures, Phys. Rev. Lett. **119**, 215701 (2017).
[17] C. Meade, R. J. Hemley, and H. K. Mao, High-Pressure X-Ray-Diffraction of SiO_2 Glass, Phys. Rev. Lett. **69**, 1387 (1992).
[18] J. F. Lin *et al.*, Electronic bonding transition in compressed SiO_2 glass, Phys. Rev. B **75**, 012201 (2007).
[19] H. Fukui, M. Kanzaki, N. Hiraoka, and Y. Q. Cai, Coordination environment of silicon in silica glass up to 74 GPa: An x-ray Raman scattering study at the silicon L edge, Phys. Rev. B **78**, 012203 (2008).
[20] C. J. Benmore, E. Soignard, S. A. Amin, M. Guthrie, S. D. Shastri, P. L. Lee, and J. L. Yarger, Structural and topological changes in silica glass at pressure, Phys. Rev. B **81**, 054105 (2010).
[21] M. Murakami and J. D. Bass, Spectroscopic Evidence for Ultrahigh-Pressure Polymorphism in SiO_2 Glass, Phys. Rev. Lett. **104**, 025504 (2010).
[22] C. Sonneville, A. Mermet, B. Champagnon, C. Martinet, J. Margueritat, D. de Ligny, T. Deschamps, and F. Balima, Progressive transformations of silica glass upon densification, J. Chem. Phys. **137**, 124505 (2012).
[23] A. Zeidler *et al.*, High-Pressure Transformation of SiO_2 Glass from a Tetrahedral to an Octahedral Network: A Joint Approach Using Neutron Diffraction and Molecular Dynamics, Phys. Rev. Lett. **113**, 135501 (2014).
[24] C. Prescher, V. B. Prakapenka, J. Stefanski, S. Jahn, L. B. Skinner, and Y. B. Wang, Beyond sixfold coordinated Si in SiO_2 glass at ultrahigh pressures, Proc. Natl. Acad. Sci. U.S.A. **114**, 10041 (2017).
[25] S. K. Lee, Y. H. Kim, Y. S. Yi, P. Chow, Y. M. Xiao, C. Ji, and G. Y. Shen, Oxygen Quadclusters in SiO_2 Glass above Megabar Pressures up to 160 GPa Revealed by X-Ray Raman Scattering, Phys. Rev. Lett. **123**, 235701 (2019).
[26] S. Petitgirard *et al.*, Magma properties at deep Earth's conditions from electronic structure of silica, Geochem. Perspect. Lett. **9**, 32 (2019).
[27] Y. Kono, Y. Shu, C. Kenney-Benson, Y. B. Wang, and G. Y. Shen, Structural Evolution of SiO_2 Glass with Si Coordination Number Greater than 6, Phys. Rev. Lett. **125**, 205701 (2020).

[28] T. Sato and N. Funamori, High-pressure structural transformation of SiO_2 glass up to 100 GPa, Phys. Rev. B **82**, 184102 (2010).
[29] M. Wu, Y. F. Liang, J. Z. Jiang, and J. S. Tse, Structure and properties of dense silica glass, Sci. Rep. **2**, 398 (2012).
[30] M. Murakami, S. Kohara, N. Kitamura, J. Akola, H. Inoue, A. Hirata, Y. Hiraoka, Y. Onodera, I. Obayashi, J. Kalikka, N. Hirao, T. Musso, A. S. Foster, Y. Idemoto, O. Sakata, and Y. Ohishi, Ultrahigh-pressure form of SiO_2 glass with dense pyrite-type crystalline homology, Phys. Rev. B **99**, 045153 (2019).
[31] J. van Straaten and I. F. Silvera, Equation of state of solid molecular H_2 and D_2 at 5 K, Phys. Rev. B **37**, 1989 (1988).
[32] R. J. Hemley, M. Hanfland, and H. K. Mao, High-pressure dielectric measurements of solid hydrogen to 170 GPa, Nature (London) **350**, 488 (1991).
[33] W. J. Evans and I. F. Silvera, Index of refraction, polarizability, and equation of state of solid molecular hydrogen, Phys. Rev. B **57**, 14105 (1998).
[34] C. S. Zha, R. J. Hemley, S. A. Gramsch, H. K. Mao, and W. A. Bassett, Optical study of H_2O ice to 120 GPa: Dielectric function, molecular polarizability, and equation of state, J. Chem. Phys. **126**, 074506 (2007).
[35] See Supplemental Material at http://link.aps.org/supplemental/10.1103/PhysRevLett.128.077403 for complete experimental and computational details, which includes Refs. [36–73].
[36] A. Dewaele, J. H. Eggert, P. Loubeyre, and R. Le Toullec, Measurement of refractive index and equation of state in dense He, H_2H_2O, and Ne under high pressure in a diamond anvil cell, Phys. Rev. B **67**, 094112 (2003).
[37] K. Syassen, Ruby under pressure, High Press. Res. **28**, 75 (2008).
[38] S. S. Lobanov, L. Schifferle, and R. Schulz, Gated detection of supercontinuum pulses enables optical probing of solid and molten silicates at extreme pressure-temperature conditions, Rev. Sci. Instrum. **91**, 053103 (2020).
[39] S. v. d. Walt, S. C. Colbert, and G. Varoquaux, The NumPy array: A structure for efficient numerical computation, Comput. Sci. Eng. **13**, 22 (2011).
[40] A. Meurer *et al.*, SymPy: Symbolic computing in Python, Peerj Comput. Sci. **3**, e103 (2017).
[41] M. I. Eremets, V. V. Struzhkin, J. A. Timofeev, I. A. Trojan, A. N. Utjuzh, and A. M. Shirokov, Refractive index of diamond under pressure, High Press. Res. **9**, 347 (1992).
[42] M. P. Surh, S. G. Louie, and M. L. Cohen, Band-gaps of diamond under anisotropic stress, Phys. Rev. B **45**, 8239 (1992).
[43] K. Katagiri, N. Ozaki, K. Miyanishi, N. Kamimura, Y. Umeda, T. Sano, T. Sekine, and R. Kodama, Optical properties of shock-compressed diamond up to 550 GPa, Phys. Rev. B **101**, 184106 (2020).
[44] A. R. Oganov, M. J. Gillan, and G. D. Price, *Ab initio* lattice dynamics and structural stability of MgO, J. Chem. Phys. **118**, 10174 (2003).
[45] D. E. Fratanduono, J. H. Eggert, M. C. Akin, R. Chau, and N. C. Holmes, A novel approach to Hugoniot measurements utilizing transparent crystals, J. Appl. Phys. **114**, 043518 (2013).
[46] R. E. Stephens and I. H. Malitson, Index of refraction of magnesium oxide, J. Res. Natl. Bur. Stand. **49**, 249 (1952).
[47] G. L. Tan, M. F. Lemon, and R. H. French, Optical properties and London dispersion forces of amorphous silica determined by vacuum ultraviolet spectroscopy and spectroscopic ellipsometry, J. Am. Ceram. Soc. **86**, 1885 (2003).
[48] G. L. Tan, M. F. Lemon, D. J. Jones, and R. H. French, Optical properties and London dispersion interaction of amorphous and crystalline SiO_2 determined by vacuum ultraviolet spectroscopy and spectroscopic ellipsometry, Phys. Rev. B **72**, 205117 (2005).
[49] R. J. Hemley, H. K. Mao, G. Y. Shen, J. Badro, P. Gillet, M. Hanfland, and D. Hausermann, X-ray imaging of stress and strain of diamond, iron, and tungsten at megabar pressures, Science **276**, 1242 (1997).
[50] B. Li, C. Ji, W. Yang, J. Wang, K. Yang, R. Xu, W. Liu, Z. Cai, J. Chen, and H.-k. Mao, Diamond anvil cell behavior up to 4 Mbar, Proc. Natl. Acad. Sci. U.S.A. **115**, 1713 (2018).
[51] H. K. Mao, J. Badro, J. F. Shu, R. J. Hemley, and A. K. Singh, Strength, anisotropy, and preferred orientation of solid argon at high pressures, J. Phys. Condens. Matter **18**, S963 (2006).
[52] D. J. Dunstan, Theory of the gasket in diamond anvil high-pressure cells, Rev. Sci. Instrum. **60**, 3789 (1989).
[53] A. K. Singh, The lattice strains in a specimen (cubic system) compressed nonhydrostatically in an opposed anvil device, J. Appl. Phys. **73**, 4278 (1993).
[54] M. Grimsditch, Annealing and relaxation in the high-pressure phase of amorphous SiO_2, Phys. Rev. B **34**, 4372 (1986).
[55] O. B. Tsiok, V. V. Brazhkin, A. G. Lyapin, and L. G. Khvostantsev, Logarithmic Kinetics of the Amorphous-Amorphous Transformations in SiO_2 and GeO_2 Glasses under High Pressure, Phys. Rev. Lett. **80**, 999 (1998).
[56] L. P. Davila, M. J. Caturla, A. Kubota, B. Sadigh, T. D. de la Rubia, J. F. Shackelford, S. H. Risbud, and S. H. Garofalini, Transformations in the Medium-Range Order of Fused Silica under High Pressure, Phys. Rev. Lett. **91**, 205501 (2003).
[57] D. Wakabayashi, N. Funamori, and T. Sato, Enhanced plasticity of silica glass at high pressure, Phys. Rev. B **91**, 014106 (2015).
[58] A. K. Singh, J. Hu, J. Shu, H. K. Mao, and R. J. Hemley, Strength of rhenium from x-ray diffraction experiments under nonhydrostatic compression to 250 GPa, J. Phys. Conf. Ser. **377**, 012008 (2012).
[59] T. Sato and N. Funamori, High-pressure *in situ* density measurement of low-Z noncrystalline materials with a diamond-anvil cell by an x-ray absorption method, Rev. Sci. Instrum. **79**, 073906 (2008).
[60] T. Sato, N. Funamori, and T. Yagi, Helium penetrates into silica glass and reduces its compressibility, Nat. Commun. **2**, 345 (2011).
[61] M. Grimsditch, Polymorphism in Amorphous SiO_2, Phys. Rev. Lett. **52**, 2379 (1984).
[62] E. H. Bogardus, Third-order elastic constants of Ge, MgO, and fused SiO_2, J. Appl. Phys. **36**, 2504 (1965).

[63] L. Peselnick, R. Meister, and W. H. Wilson, Pressure derivatives of elastic moduli of fused quartz to 10 kb, J. Phys. Chem. Solids **28**, 635 (1967).
[64] K. Kondo, S. Iio, and A. Sawaoka, Nonlinear pressure dependence of the elastic moduli of fused quartz up to 3 GPa, J. Appl. Phys. **52**, 2826 (1981).
[65] D. Wakabayashi, N. Funamori, T. Sato, and T. Taniguchi, Compression behavior of densified SiO_2 glass, Phys. Rev. B **84**, 144103 (2011).
[66] C. Z. Tan and J. Arndt, The mean polarizability and density of glasses, Physica (Amsterdam) **229B**, 217 (1997).
[67] P. Hohenberg and W. Kohn, Inhomogeneous electron gas, Phys. Rev. **136**, B864 (1964).
[68] S. J. Clark, M. D. Segall, C. J. Pickard, P. J. Hasnip, M. J. Probert, K. Refson, and M. C. Payne, First principles methods using CASTEP, Z. Kristallogr. **220**, 567 (2005).
[69] J. P. Perdew, K. Burke, and M. Ernzerhof, Generalized Gradient Approximation Made Simple, Phys. Rev. Lett. **77**, 3865 (1996).
[70] K. Lejaeghere *et al.*, Reproducibility in density functional theory calculations of solids, Science **351**, 1415 (2016).
[71] H. J. Monkhorst and J. D. Pack, Special points for brillouin-zone integrations, Phys. Rev. B **13**, 5188 (1976).
[72] K. Refson, P. R. Tulip, and S. J. Clark, Variational density-functional perturbation theory for dielectrics and lattice dynamics, Phys. Rev. B **73**, 155114 (2006).
[73] K. Klier, J. A. Spirko, and K. M. Landskron, Optical absorption anisotropy of high-density, wide-gap, high-hardness SiO_2 polymorphs seifertite, stishovite, and coesite, Am. Mineral. **100**, 120 (2015).
[74] E. Hecht, *Optics*, 5th ed. (Pearson Education, Inc., London, 2017), p. 714.
[75] C. S. Zha, R. J. Hemley, H. K. Mao, T. S. Duffy, and C. Meade, Acoustic velocities and refractive index of SiO_2 glass to 57.5 GPa by Brillouin scattering, Phys. Rev. B **50**, 13105 (1994).
[76] I. H. Malitson, Interspecimen comparison of the refractive index of fused silica, J. Opt. Soc. Am. **55**, 1205 (1965).
[77] Y. Akahama and H. Kawamura, High-pressure Raman spectroscopy of diamond anvils to 250 GPa: Method for pressure determination in the multimegabar pressure range, J. Appl. Phys. **96**, 3748 (2004).
[78] T. Deschamps, A. Kassir-Bodon, C. Sonneville, J. Margueritat, C. Martinet, D. de Ligny, A. Mermet, and B. Champagnon, Permanent densification of compressed silica glass: A Raman-density calibration curve, J. Phys. Condens. Matter **25**, 025402 (2013).
[79] M. Guerette, M. R. Ackerson, J. Thomas, F. L. Yuan, E. B. Watson, D. Walker, and L. P. Huang, Structure and properties of silica glass densified in cold compression and hot compression, Sci. Rep. **5**, 15343 (2015).
[80] N. M. Trease, T. M. Clark, P. J. Grandinetti, J. F. Stebbins, and S. Sen, Bond length-bond angle correlation in densified silica-results from ^{17}O NMR spectroscopy, J. Chem. Phys. **146**, 184505 (2017).
[81] S. Bruns, T. Uesbeck, S. Fuhrmann, M. T. Aymerich, L. Wondraczek, D. de Ligny, and K. Durst, Indentation densification of fused silica assessed by Raman spectroscopy and constitutive finite element analysis, J. Am. Ceram. Soc. **103**, 3076 (2020).
[82] V. Keryvin, J. X. Meng, S. Gicquel, J. P. Guin, L. Charleux, J. C. Sangleboeuf, P. Pilvin, T. Rouxel, and G. Le Quilliec, Constitutive modeling of the densification process in silica glass under hydrostatic compression, Acta Mater. **62**, 250 (2014).
[83] S. H. Wemple and M. DiDomenico, Behavior of the electronic dielectric constant in covalent and ionic materials, Phys. Rev. B **3**, 1338 (1971).
[84] R. E. Cohen, Bonding and elasticity of stishovite SiO_2 at high pressure: Linearized augmented plane wave calculations, Am. Mineral. **76**, 733 (1991), https://pubs.geoscienceworld.org/msa/ammin/article/76/5-6/733/105119/Bonding-and-elasticity-of-stishovite-SiO2-at-high.
[85] E. Bykova *et al.*, Metastable silica high pressure polymorphs as structural proxies of deep Earth silicate melts, Nat. Commun. **9**, 4789 (2018).
[86] D. A. Keen and M. T. Dove, Local structures of amorphous and crystalline phases of silica, SiO_2, by neutron total scattering, J. Phys. Condens. Matter **11**, 9263 (1999).
[87] L. P. Huang and J. Kieffer, Amorphous-amorphous transitions in silica glass. I. Reversible transitions and thermomechanical anomalies, Phys. Rev. B **69**, 224203 (2004).
[88] S. Petitgirard, W. J. Malfait, R. Sinmyo, I. Kupenko, L. Hennet, D. Harries, T. Dane, M. Burghammer, and D. C. Rubie, Fate of $MgSiO_3$ melts at core-mantle boundary conditions, Proc. Natl. Acad. Sci. U.S.A. **112**, 14186 (2015).
[89] S. Petitgirard, G. Spiekermann, K. Glazyrin, J. Garrevoet, and M. Murakami, Density of amorphous GeO_2 to 133 GPa with possible pyritelike structure and stiffness at high pressure, Phys. Rev. B **100**, 214104 (2019).